J|A|C|S
ARTICLES
Published on Web 12/13/2001

Cu(II)-Mediated Intramolecular Carbene Cation Radical Formation: Relevance to Unimolecular Metal−Ligand Radical Intermediates

Brian J. Kraft, Hilary J. Eppley, John C. Huffman, and Jeffrey M. Zaleski*

Contribution from the Department of Chemistry and Molecular Structure Center, Indiana University, Bloomington, Indiana 47405

Received August 20, 2001

Abstract: We report the syntheses of the photochemically labile 9-diazo-4,5-diazafluorene (**1**) framework and the corresponding Cu(9-diazo-4,5-diazafluorene)$_2$(NO$_3$)$_2$ compound (**2**). The X-ray structure of **2** reveals a 6-coordinate, tetragonal geometry with one nitrogen donor of an asymmetrically chelated diazafluorene in the equatorial position and the other defining the weak Jahn−Teller axis. The nitrate counterions bind in a monodentate fashion in the equatorial plane to complete the coordination sphere. Extended Hückel calculations reveal that the unusual solid-state structure derives from the enlarged bite angle of the fluorene skeleton and steric interactions between the adjacent hydrogen atoms in the higher energy (0.45 eV) symmetrically coordinated state. This is in contrast to Cu(py)$_4$(NO$_3$)$_2$ which is 1.3 eV more stable with the nitrate counterions bound along the Jahn−Teller axis. Electron paramagnetic resonance (EPR) studies in solution reveal that the nitrates dissociate to yield 6-coordinate CuN$_2$X$_2$N$_2'$ structures with either a bound chloride ion ($g_x = 2.10$, $g_y = 2.04$, $g_z = 2.23$, $A_z = 177 \times 10^{-4}$ cm^{-1}) or a mixture of counterion and solvent ($g_{xa} = 2.05$, $g_{ya} = 2.06$, $g_{za} = 2.29$, $A_{za} = 170 \times 10^{-4}$ cm^{-1}; $g_{xb} = 2.07$, $g_{yb} = 2.08$, $g_{zb} = 2.34$, $A_{zb} = 155 \times 10^{-4}$ cm^{-1}). Photolyses of **1** and **2** indicate loss of N$_2$ and formation of either carbene ($|D/hc| = 0.408$ cm^{-1}, $|E/hc| = 0.0292$ cm^{-1}) or Cu(I)−L$^{\bullet+}$ ($S = {}^1/_2$, $g = 2.0019$) intermediates, which are identified by EPR, UV−vis, and time-dependent density functional theory methods. The results illustrate the important role redox active transition metals play in determining the nature of fundamental metal−ligand radical intermediates.

Introduction

Diazo compounds are known to release dinitrogen upon thermal and photochemical activation to produce unstable carbene intermediates that react with a variety of substrates.[1−3] The facile reactivities of these highly energetic compounds have long been exploited by organic chemists to facilitate various transformations such as C−H bond insertion, double bond addition, and double H-atom abstraction.[1,3] Recently, the reactivities of organic diazo compounds have also shown potential in a variety of applied fields, including the generation of lithographic resists, light-sensitive varnish used in the processing of silicon chips, for the electronics industry.[4,5] Diazo compounds also have biologically relevant applications including their use in structural biology as radioactive photoaffinity labels,[6−9] photofootprinting agents,[10,11] as well as potential antitumor agents in medicinal chemistry.[12−15]

The decomposition of diazo groups is known to be facilitated by the presence of both oxidizing and reducing agents.[16] Consequently, their reactivities may be enhanced by interaction with transition metals in either high or low oxidation states. To this end, both Cu(I) complexes and salts have been used extensively in organic syntheses to catalyze decomposition of the diazo unit for C−C coupling reactions including addition, insertion, and the synthesis of ylides.[3] Diazo compounds have also been used as reducing agents for Cu(II) salts to generate catalytically active Cu(I) species in situ.[3] This redox partnership presents opportunities for generating an inter- or intramolecular

* To whom correspondence should be addressed. E-mail: zaleski@indiana.edu.

(1) Regitz, M.; Maas, G. *Diazo Compounds: Properties and Synthesis*; Academic Press: Orlando, 1986.
(2) Ando, W. *Photochemistry of the Diazonium and Diazo Groups*; Wiley & Sons: New York, 1978; Vol. 1, pp 341−487.
(3) Doyle, M. P.; McKervey, M. A.; Ye, T. *Modern Catalytic Methods for Organic Synthesis with Diazo Compounds: From Cyclopropanes to Ylides*; Wiley: New York, 1998.
(4) Reiser, A.; Shih, H.-Y.; Yeh, T.-F.; Huang, J.-P. *Angew. Chem., Int. Ed. Engl.* **1996**, *35*, 2429−2440.
(5) Wallraff, G. M.; Hinsberg, W. D. *Chem. Rev.* **1999**, *99*, 1801−1821.
(6) Blanton, M. P.; Dangott, L. J.; Raja, S. K.; Lala, A. K.; Cohen, J. B. *J. Biol. Chem.* **1998**, *273*, 8659−8668.
(7) Fagart, J.; Sobrio, F.; Marquet, A. *J. Labelled Compd. Radiopharm.* **1997**, *39*, 791−795.
(8) Pandurangi, R. S.; Lusiak, P.; Kuntz, R. R.; Volkert, W. A.; Rogowski, J.; Platz, M. S. *J. Org. Chem.* **1998**, *63*, 9019−9030.
(9) Rak, S. F.; Schuster, G. B. *Photochem. Photobiol.* **1987**, *45*, 439−443.
(10) Jeppesen, C.; Nielsen, P. E. *Eur. J. Biochem.* **1989**, *182*, 437−444.
(11) Nakatani, K.; Shirai, J.; Sando, S.; Saito, I. *Tetrahedron Lett.* **1997**, *38*, 6047−6050.
(12) Wu, F.; Bergstrom, M.; Stridsberg, M.; Orlefors, H.; Eriksson, B.; Oberg, K.; Watanabe, Y.; Langstrom, B. *Anticancer Res.* **1997**, *17*, 2363−2367.
(13) Nakatani, K.; Maekawa, S.; Tanabe, K.; Saito, I. *J. Am. Chem. Soc.* **1995**, *117*, 10635−10644.
(14) Hiramoto, K.; Kaku, M.; Sueyoshi, A.; Fujise, M.; Kikugawa, K. *Chem. Res. Toxicol.* **1995**, *8*, 356−362.
(15) Daidone, G.; Maggio, B.; Plescia, S.; Raffa, D.; Musiu, C.; Milia, C.; Perra, G.; Marongiu, M. E. *Eur. J. Med. Chem.* **1998**, *35*, 375−382.
(16) Bethell, D.; Parker, V. D. *Acc. Chem. Res.* **1988**, *21*, 400−407.

10.1021/ja0120072 CCC: $22.00

redox switch given the recent interest in radical cations derived from diaryl diazo compounds.[17−20]

In addition to the chemical reactivity of diazo compounds with redox active metals, the geometric and electronic structural characteristics of metals such as paramagnetism, optical absorption and emission properties, and radioactivity may enhance the usefulness of these highly reactive agents for applications in materials science, medicine, and biochemistry. For example, transient magnetic materials have been prepared from metal−diazo coordination polymers whose ground-state paramagnetic signatures can be photochemically modulated by production of a ligand-localized diradical that couples to the spin on the metal center.[21,22] The importance of metal−ligand radical intermediates, however, is not restricted to applications in synthesis[3] and materials,[23,24] but extends to DNA degradation agents[25−27] and general bioinorganic chemistry[28−31] as well. Here, the emerging role of metal−ligand radical intermediates for storing redox equivalents during metalloenzyme activity[29,32−34] (e.g., galactose oxidase) further underscores the importance of fundamental redox active metal−ligand radical chemistry.

Our interests lie in the function of metal ions in the determination of the fundamental chemical intermediates produced upon photolysis of metal−diazo compounds with relevance to materials science and bioinorganic chemistry. Toward these goals, we have synthesized and structurally characterized the thermally and photochemically labile 9-diazo-4,5-diazafluorene (**1**) framework and the corresponding Cu(9-diazo-4,5-diazafluorene)$_2$(NO$_3$)$_2$ compound (**2**). Comparison of the photochemical reactivities of **1** and **2** using low-temperature electron paramagnetic resonance (EPR) and electronic absorption spectroscopies reveals that the Cu(II) center strongly influences the electronic structure of the photogenerated radical intermediates.

Experimental Section

Physical Measurements. Samples were prepared using volumetric glassware and standard Schlenk and drybox techniques. Solvents were degassed either by purging with N_2 for >1 h or by several freeze-pump thaw cycles. ^{1}H NMR spectra were collected on a 300 MHz Varian Gemini 2000 NMR spectrometer with the proton solvent as a reference. Elemental analyses were performed by the Atlantic Microanalytical Laboratory at Norcross, GA, or at Indiana University using a Perkin-Elmer Series II CHNS/O Analyzer 2400. Infrared spectra were recorded either as KBr pellets or in a fluorolube mull on a Nicolet 510P spectrophotometer. Cyclic voltammograms and differential pulse voltammograms were recorded on a BAS CV-50W voltametric analyzer. A three-electrode assembly utilizing a glassy carbon working electrode, a platinum auxiliary electrode, and an SCE reference electrode was employed without the application of IR compensation. Conductivity measurements were made using a YSI Model 31A conductance bridge and a YSI Model 3403 conductivity cell (1 cm^{-1} cell constant). Electronic absorption spectra were collected on a Perkin-Elmer Lambda 19 UV/VIS/NIR spectrometer at ambient temperature. Low-temperature electronic spectral measurements were performed in an Oxford Instruments optical cryostat, which was mounted directly inside the spectrometer. Fluorescence measurements were obtained with a Perkin-Elmer LS 50 B luminescence spectrometer equipped with a Hamatatsu model R2371 PMT. Quantum yields are given for solutions of matched optical density at the excitation wavelength and are reported relative to the fluorescence of phenol. All electron paramagnetic resonance spectra were recorded at X-band (9.5 GHz) on an ESP 300 Bruker instrument. Typical EPR conditions: microwave power, 10 mW; modulation amplitude, 2−20 G; modulation frequency, 100 kHz; receiver gain, $(2-5) \times 10^4$. EPR spectra were simulated using SimFonia (Bruker) for organic radicals and a Monte Carlo method for the copper signals.[35,36] Matrix photolyses were performed directly in the EPR cavity and the optical dewar with a 150 W Hg source coupled via a liquid light pipe (Oriel # 77557). Photolyses were run with $\lambda \geq 455$ nm, where the cutoff wavelength was selected using a series of long wavelength pass filters (345, 420, and 455 nm). Photolyses at $\lambda = 457$ nm and $\lambda = 647$ nm were performed with Ar^+ and Kr^+ ion lasers (Coherent models I-70 and I-300), respectively, using powers of ≅300 mW. Solid-state photolyses were performed with a 1000 W Xe lamp and long pass filters (295, 345, 420, 455 nm) at 20 °C.

Synthetic Methods. All synthetic preparations were performed under ambient oxygen conditions. Reagents were used as received without further purification, and all solvents used were spectrochemical grade. The starting material, 4,5-diazafluorenone-9-hydrazone, was synthesized from the aqueous oxidation of 1,10-phenathroline followed by the formation of the hydrazone using hydrazine hydrate, according to literature procedures.[37−39] ***Caution.*** *Diazo compounds are highly reactive and produce copious amounts of N_2 gas upon photo- or thermal decomposition. Although we did not witness the detonation of solid samples of these compounds, adequate precautions should be taken when working with them.*

Synthesis of 9-Diazo-4,5-diazafluorene (1). 4,5-Diazafluorenone-9-hydrazone (1.0 g, 5.1 mmol) was oxidized using a basic solution (10 drops of saturated KOH in water) of yellow HgO (1.2 g, 5.5 mmol) in benzene (200 mL). The solution was stirred overnight at room temperature and then filtered through glass wool or filter paper to remove the insoluble Hg waste. The resulting orange solution was concentrated to a solid and then recrystallized from a mixture of dichloromethane and pentane at −20 °C. Yield: 52−65%. Anal. Calcd for $C_{11}H_6N_4$: C, 67.71; H, 2.97; N, 24.28. Found: C, 67.73; H, 3.11; N, 24.32. EI MS *m*/*z*: 194.1 (M^+), 166.1 ($M^+ - N_2$). ^{1}H NMR ($CDCl_3$): δ ppm 8.72 (dd, 2H, $J = 1.5$, 4.7 Hz), 7.91 (dd, 2H, $J = 1.5$, 8.0 Hz), 7.39 (dd, 2H, $J = 4.7$, 8.0 Hz). Selected IR data (KBr, cm^{-1}): 3040 (w), 2060 (vs), 1718 (w), 1593 (w), 1560 (w), 1545 (w), 1410

(17) Ishiguro, K.; Ikeda, M.; Sawaki, Y. *J. Org. Chem.* **1992**, *57*, 3057−3066.
(18) Bally, T.; Carra, C.; Matzinger, S.; Truttmann, L.; Gerson, F.; Schmidlin, R.; Platz, M. S.; Admasu, A. *J. Am. Chem. Soc.* **1999**, *121*, 7011−7019.
(19) Stoub, D. G.; Goodman, J. L. *J. Am. Chem. Soc.* **1997**, *119*, 11110−11111.
(20) Bally, T.; Matzinger, S.; Truttman, L.; Platz, M. S.; Admasu, A.; Gerson, F.; Arnold, A.; Schmidlin, R. *J. Am. Chem. Soc.* **1993**, *115*, 7007−7008.
(21) Koga, N.; Ishimaru, Y.; Iwamura, H. *Angew. Chem., Int. Ed. Engl.* **1996**, *35*, 755−757.
(22) Sano, Y.; Tanaka, M.; Koga, N.; Matsuda, K.; Iwamura, H.; Rabu, P.; Drillon, M. *J. Am. Chem. Soc.* **1997**, *119*, 8246−8252.
(23) Fujita, W.; Awaga, K. *J. Am. Chem. Soc.* **2001**, *123*, 3601−3602.
(24) Sakane, A.; Kumada, H.; Karasawa, S.; Koga, N.; Iwamura, H. *Inorg. Chem.* **2000**, *39*, 2891−2896.
(25) Maurer, T. D.; Kraft, B. J.; Lato, S. M.; Ellington, A. D.; Zaleski, J. M. *Chem. Commun.* **2000**, 69−70.
(26) Kraft, B. J.; Zaleski, J. M. *New J. Chem.* **2001**, *25*, 1281−1289.
(27) Eppley, H. J.; Lato, S. A.; Ellington, A. D.; Zaleski, J. M. *Chem. Commun.* **1999**, 2405−2406.
(28) Itoh, S.; Kumei, H.; Nagatomo, S.; Kitagawa, T.; Fukuzumi, S. *J. Am. Chem. Soc.* **2001**, *123*, 2165−2175.
(29) Himo, F.; Eriksson, L. A.; Maseras, F.; Siegbahn, P. E. M. *J. Am. Chem. Soc.* **2000**, *122*, 8031−8036.
(30) Kimura, S.; Bill, E.; Bothe, E.; Weyhermueller, T.; Wieghardt, K. *J. Am. Chem. Soc.* **2001**, *123*, 6025−6039.
(31) Penkert, F. N.; Weyhermueller, T.; Bill, E.; Hildebrandt, P.; Lecomte, S.; Wieghardt, K. *J. Am. Chem. Soc.* **2000**, *122*, 9663−9673.
(32) Halfen, J. A.; Jazdzewski, B. A.; Mahapatra, S.; Berreau, L. M.; Wilkinson, E. C.; Que, L. J.; Tolman, W. B. *J. Am. Chem. Soc.* **1997**, *119*, 8217−8227.
(33) Wachter, R. M.; Branchaud, B. P. *Biochim. Biophys. Acta* **1998**, *1384*, 43−54.
(34) Gerfen, G. J.; Bellew, B. F.; Griffin, R. G.; Singel, D. J.; Ekberg, C. A.; Whittaker, J. W. *J. Phys. Chem.* **1996**, *100*, 16739−16748.
(35) Neese, F. *QCPE Bull.* **1995**, *15*, 5.
(36) Gaffney, B. J.; Silverstone, H. J. In *Biological Magnetic Resonance*; Reuben, J., Berliner, J., Eds.; Plenum Press: New York, 1993; Vol. 13, p 1.
(37) Abdel-Wahab; A. A. M.; Ismail, M. T.; Mohamed, O. S.; Durr, H.; Ma, Y. M. *Liebigs Ann./Recl.* **1997**, 1611−1618.
(38) Arduengo, A. J., III; Dias, H. V. R.; Harlow, R. L.; Kline, M. *J. Am. Chem. Soc.* **1992**, *114*, 5530−5534.
(39) Mlochowski, J.; Szulc, Z. *Pol. J. Chem.* **1983**, *57*, 33−39.

(s), 1394 (s), 1336 (w), 1319 (w), 1296 (m), 1262 (m), 1202 (m), 1186 (s), 1138 (w), 1099 (w), 1065 (m), 1030 (m), 801 (s), 742 (s), 702 (w), 679 (w), 625 (w), 571 (w), 489 (w), 441 (w).

Synthesis of Bis(9-diazo-4,5-diazafluorene)copper(II) Nitrate (2). 9-Diazo-4,5-diazafluorene (76 mg, 0.39 mmol) was dissolved in 15 mL of methanol under low light conditions. The salt $Cu(NO_3)_2 \cdot 2.5H_2O$ (46 mg, 0.20 mmol) was dissolved in 5 mL of methanol. Both solutions were filtered through glass wool to remove any undissolved solid, and the $Cu(NO_3)_2$ solution was added to the ligand solution dropwise. The solution turned from orange to deep green in color and was allowed to stir for about 1 min. The reaction mixture was then allowed to stand at 4 °C for 12 h. The solution was subsequently filtered to remove the microcrystalline green solid and washed with several portions of methanol. Using a more dilute solution, crystals suitable for X-ray crystallographic analysis could be obtained directly from the reaction mixture. The solid was dried in vacuo for 2 h. Yield: 94 mg, 82% based on Cu. Anal. Calcd for $C_{22}H_{12}N_{10}O_6Cu$: C, 45.90; H, 2.02; N, 24.28. Found: C, 45.87; H, 2.10; N, 24.32. Selected IR data (KBr, cm^{-1}): 2081 (vs), 1589 (w), 1651 (w), 1466 (s), 1419 (m), 1396 (s), 1346 (w), 1262 (s), 1219 (w), 1188 (m), 1072 (w), 1013 (m), 802 (m), 731 (m), 684 (w), 644 (m), 571 (w), 486 (w), 432 (w).

X-ray Crystallographic Analysis of 2. Data for **2** were collected on a Picker four-circle goniostat equipped with a Furnas monochromator (HOG crystal), modified by addition of stepping motors (Slo-Syn) on each of the four axes, and a fifth motor driving a 20-position filter/attenuator wheel. The diffractometer control software, PCPS.EXE, was written by W. E. Streib of the IUMSC. The software for structure solution and refinement include SHELXTL-PC, and other versions of SHELX, as well as the XTEL program library. A typical, well-defined blue-green crystal was removed from the crystallization media and transferred to the goniostat where it was cooled in the gaseous nitrogen cold stream. A systematic search of a limited hemisphere of reciprocal space was used to determine that the crystal possessed no symmetry or systematic absences, corresponding to one of the triclinic space groups. Subsequent solution and refinement confirmed the centrosymmetric choice, $P\bar{1}$. The data were collected using a standard moving crystal-moving detector technique with fixed backgrounds at each extreme of the scan. The data were corrected for Lorentz, and polarization effects and equivalent reflections were averaged. The structure was readily solved using direct methods (MULTAN78) and Fourier techniques. Hydrogen atoms were readily located in a difference Fourier phased on the non-hydrogen atoms. Hydrogen atoms were assigned isotropic thermal parameters and allowed to vary for the final cycles of refinement. A final difference Fourier was featureless; the largest peak of intensity was at 0.65 e/Å^3. Atomic coordinates, bond lengths, and bond angles have been deposited at the Cambridge Crystallographic Data Center and are available as Supporting Information.

Computational Methods. Extended Hückel molecular orbital (EHMO) calculations of **2** were performed using an internal coordinates Z-matrix derived from the X-ray crystal structure Cartesian coordinates. The structure of the complex was modified to increase the short C−H bonds to at least 0.8 Å using Chem 3-D Pro. Cartesian coordinates of a comparison complex, $Cu(py)_4(NO_3)_2$ (py = pyridine), were obtained through the Cambridge Crystallographic Database, and H-atoms were added to its structure in Chem 3-D Pro. Both molecules were oriented such that their Jahn−Teller (JT) axes were positioned along the *z*-axis in the ground-state structure. Dummy atoms defining a vector that bisects the chelate bite in **2** were added as the rotation/translation axis. Extended Hückel calculations and molecular orbital visualization were performed using WINCACAO. The Hückel constant (β) was set to 1.75.

Geometry optimization for fluorenylidene was performed under a C_{2v} symmetry constraint with density functional theory (DFT) and the UB3LYP combination of functionals using the 6-31G** basis set employed in Gaussian 98.[40] A scaling factor appropriate for the method and 6-31G** basis set (0.9613)[41] was applied to the vibrational frequencies obtained from the frequency analysis at the optimized geometry. Time-dependent DFT (TDDFT) calculations were then performed with the same functionals and basis set at the optimized C_{2v} geometry to obtain electronic transition energies.

Scheme 1. Synthesis of 9-Diazo-4,5-diazafluorene (**1**) and the Corresponding Cupric Complex (**2**)

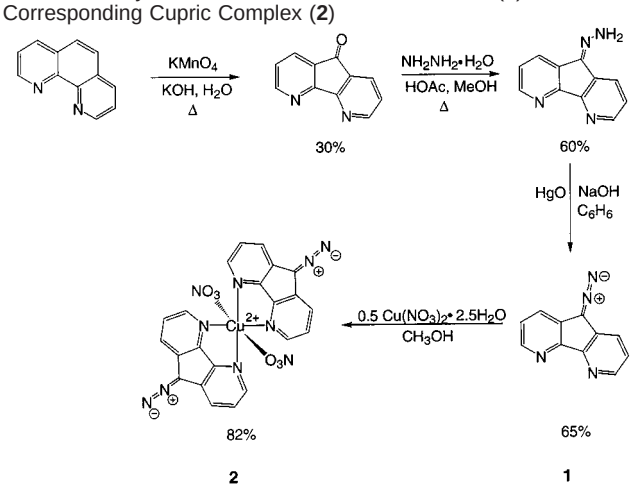

Results

Syntheses. The solubility of metal−diazo complexes has been an impediment to the development of molecular-based applications of metal−diazo compounds. Polymeric diazo structures are common among the previous examples of metal-coordinated diazo compounds.[21,22] For our studies, a simple chelating ligand with an exocyclic diazo group was desired because it minimizes potential polymeric interactions among multiple metal centers. Although the 9-diazo-4,5-diazafluorene ligand (**1**) has been used in the synthesis of extended organic arrays for molecular racks (MOLRACs)[42] through chemistry at the diazo group, it has not been utilized previously as an independent ligand.

Compound **1** was synthesized from 4,5-diazafluorenone, using modified literature procedures.[37−39] Briefly, 1,10-phenanthroline is oxidized under basic conditions to form the 4,5-diazafluorene. The 4,5-diazafluorenone-9-hydrazone was then prepared by addition of excess hydrazine hydrate, and subsequent oxidation with yellow HgO yields 9-diazo-4,5-diazafluorene (Scheme 1). The copper(II) complex, bis(9-diazo-4,5-diazafluorene)Cu(II)-$(NO_3)_2$ (**2**), was then synthesized by adding a methanolic solution of $Cu(NO_3)_2 \cdot 2.5H_2O$ to a solution of ligand in a 1:2 ratio in the dark. Green microcrystals of **2** precipitated out of this solution immediately and could be isolated by filtration in the dark. Larger, X-ray quality crystals were grown directly from a more dilute reaction solution.

(40) Frisch, M. J.; Trucks, G. W.; Schlegel, H. B.; Scuseria, G. E.; Robb, M. A.; Cheeseman, J. R.; Zakrzewski, V. G.; Montgomery, J. A., Jr.; Stratmann, R. E.; Burant, J. C.; Dapprich, S.; Millam, J. M.; Daniels, A. D.; Kudin, K. N.; Strain, M. C.; Farkas, O.; Tomasi, J.; Barone, V.; Cossi, M.; Cammi, R.; Mennucci, B.; Pomelli, C.; Adamo, C.; Clifford, S.; Ochterski, J.; Petersson, G. A.; Ayala, P. Y.; Cui, Q.; Morokuma, K.; Malick, D. K.; Rabuck, A. D.; Raghavachari, K.; Foresman, J. B.; Cioslowski, J.; Ortiz, J. V.; Stefanov, B. B.; Liu, G.; Liashenko, A.; Piskorz, P.; Komaromi, I.; Gomperts, R.; Martin, R. L.; Fox, D. J.; Keith, T.; Al-Laham, M. A.; Peng, C. Y.; Nanayakkara, A.; Gonzalez, C.; Challacombe, M.; Gill, P. M. W.; Johnson, B. G.; Chen, W.; Wong, M. W.; Andres, J. L.; Head-Gordon, M.; Replogle, E. S.; Pople, J. A. *Gaussian 98*, revision A.6; Gaussian, Inc.: Pittsburgh, PA, 1998.
(41) Foresman, J. B.; Frisch, A. *Exploring Chemistry with Electronic Structure Methods*, 2nd ed.; Gaussian: Pittsburgh, 1993.
(42) Warrener, R. N.; Ferreira, A. B. B.; Schultz, A. C.; Butler, D. N.; Keene, F. R.; Kelso, L. S. *Angew. Chem., Int. Ed. Engl.* **1996**, *35*, 2485−2487.

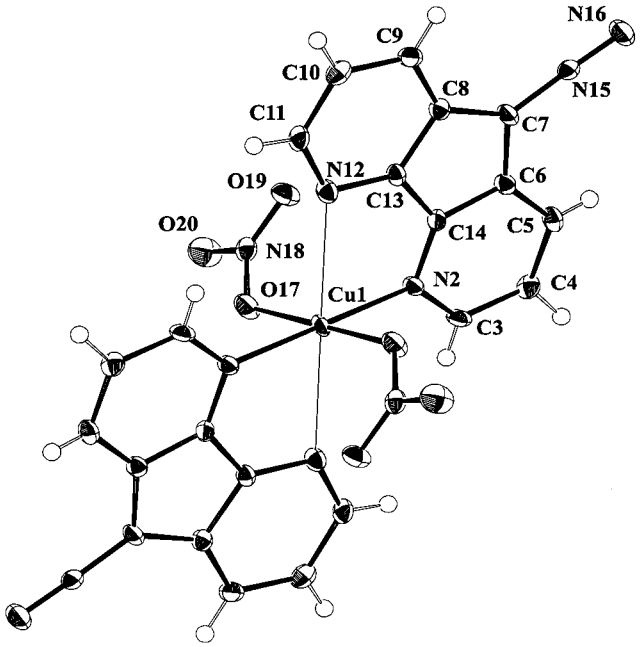

Figure 1. ORTEP of the X-ray crystal structure of **2**. Thermal ellipsoids are illustrated at 50% probability.

Table 1. Crystallographic Data for **2**

empirical formula	$C_{22}H_{12}N_{10}O_6Cu$
formula weight	575.95
color of crystal	green
crystal system	triclinic
space group	$P\bar{1}$
a, Å	8.897(4)
b, Å	10.178(5)
c, Å	6.833(3)
α, deg	104.47(2)
β, deg	103.31(2)
γ, deg	109.22(2)
V, Å^3	531.68
Z	1
T, K	105
λ, Å	0.71069
ρ_{calcd}, g/cm^3	1.799
μ, cm^{-1}	10.970
$R(F_o)^a$	0.0389
$R_w(F_o)^b$	0.0356
GOF	1.508

^{a} $R = \sum||F_o| - |F_c||/\sum|F_o|$. ^{b} $R_w = [\sum w(|F_o| - |F_c|)^2/\sum w|F_o|^2]^{1/2}$, where $w = 1/\sigma^2(|F_o|)$.

Solid State Characterization. X-ray Crystal Structure. An ORTEP diagram of **2** is shown in Figure 1, and the compound's crystallographic data are given in Table 1. While the unit cell is composed of only one molecule, stacking of the cells in the *z*-direction results in a two-dimensional arrangement of columns with an interccolumnar separation of 6.83 Å. No close intermolecular hydrogen-bonding contacts are evident in the crystal structure. The closest contact (2.99 Å) involves diazo groups between two neighboring unit cells.

The molecular structure of **2** (Figure 1, Table 2) is one of a relatively small group of metal complexes with diazafluorene-type ligands, which includes diazafluorenes,[43−46] diazafluorenones,[47] and diazafluorenone hydrazone.[48,49] It is also the first inorganic structure in this family to possess a thermally and photochemically reactive diazo group at the 9-position of the fluorene skeleton. The coordination geometry of **2** is unusual in that the elongated J−T axis of the molecule lies along the N−Cu−N vector (Cu(1)−N(12) = 2.651 Å) and not in the O−Cu−O axis (Cu(1)−O(12) = 2.014 Å, O(17)−Cu(1)−O(17) = 179.96°), which is occupied by nitrate counterions. To our knowledge, this is one of only two examples of $N_2O_2N_2'$ coordination to a Cu(II) center with two *nitrates* bound trans in the equatorial plane and the nitrogens of the chelate directed along the J−T axis.[50] This $N_2X_2N_2'$ geometry has been observed in other Cu(II) complexes with the 4,5-diazafluorene template and simple anions such as Cl^- or Br^-,[50] while complexes with transition metals other than Cu(II) (e.g., Re(I),[51] Ni(II),[52] Co(II)[48]) typically exhibit a more symmetrical coordination. Although there is no analogous structure to **2** for comparison of the distances within the diazo group, the N═N (1.136 Å) and N═C (1.319 Å) bond lengths are similar to the crystallographically characterized 9-diazofluorene.[53]

Table 2. Selected Bond Distances (Å) and Angles (deg) for **2**

Cu(1)−O(17)	2.014(3)	N(2)−Cu(1)−N(12)	79.69(10)
Cu(1)−N(2)	1.982(3)	Cu(1)−O(17)−N(18)	126.33(19)
Cu(1)−N(12)	2.651(3)	Cu(1)−N(2)−C(3)	129.20(22)
N(15)−C(7)	1.319(4)	Cu(1)−N(2)−C(14)	113.33(22)
N(15)−N(16)	1.136(4)	Cu(1)−N(12)−C(11)	150.83(22)
O(17)−N(18)	1.292(3)	Cu(1)−N(12)−C(13)	94.17(19)
O(17)−Cu(1)−O(17)	180.00	N(16)−N(15)−C(7)	178.5(3)
O(17)−Cu(1)−N(2)	85.18(10)	N(15)−C(7)−C(8)	126.6(3)
O(17)−Cu(1)−N(2)^a	94.82(10)	O(17)−N(18)−O(19)	120.41(27)
O(17)−Cu(1)−N(12)	99.31(9)		

^{a} $(x - 1, y - 1, z - 1)$.

Extended Hückel Calculations. Extended Hückel molecular orbital (EHMO) calculations were performed on **1** and **2** to provide general insight into the origin of the unusual coordination geometry and to investigate the electronic structure of the copper complex. Figure 2 reveals the frontier molecular orbitals for both **1** and **2** and their relative energies. For **1**, two nearly degenerate orbitals primarily localized on the diazo unit are observed. The HOMO is *π*-bonding relative to the C═N bond at the 9-position and nonbonding between the nitrogens within the N═N unit. The two lowest energy unfilled MOs localized on the diazo unit are both C═N nonbonding and N═N *π*-antibonding, consistent with the propensity for N_2 loss via the electronic transition between these orbitals ($n \rightarrow \pi^*$). For **2**, the ligand orbitals are of very similar parentage, but the half-filled, primarily $d_{x^2-y^2}$ metal-based orbital is now formally the HOMO as it lies energetically ∼0.3 eV above the filled orbitals localized on the ligands.

(43) Thummel, R. P.; Lefoulon, F.; Korp, J. D. *Inorg. Chem.* **1987**, *26*, 2370−2376.
(44) Witte, P. T.; Klein, R.; Kooijman, H.; Spek, A. L.; Polasek, M.; Varga, V.; Mach, K. *J. Organomet. Chem.* **1996**, *519*, 195−204.
(45) Henderson, L. J., Jr.; Fronczek, F. R.; Cherry, W. R. *J. Am. Chem. Soc.* **1984**, *106*, 5876−5879.
(46) Klein, R. A.; van Belzen, R.; Vrieze, K.; Elsevier, C. J.; Thummel, R. P.; Fraanje, J.; Goubitz, K. *Collect. Czech. Chem. Commun.* **1997**, *62*, 238−256.
(47) Balagopalakrishna, C.; Rajasekharan, M. V.; Bott, S.; Atwood, J. L.; Ramakrishna, B. L. *Inorg. Chem.* **1992**, *31*, 2843−2846.
(48) Shi, X.-H.; You, X.-Z.; Li, C.; Xiong, R.-G.; Yu, K.-B. *Transition Met. Chem.* **1995**, *20*, 191−195.
(49) Lu, Z.-L.; Duan, C.-Y.; Tian, Y.-P.; You, X.-Z.; Fun, H.-K.; Yip, B.-C.; Hovestreydt, E. *Polyhedron* **1996**, *16*, 187−194.
(50) Menon, S.; Rajasekharan, M. V. *Polyhedron* **1998**, *17*, 2463−2476.
(51) Yam, V. W.-W.; Wang, K.-Z.; Wang, C.-R.; Yang, Y.; Cheung, K.-K. *Organometallics* **1998**, *17*, 2440−2446.
(52) Xiong, R.-G.; Zuo, J.-L.; Xu, E.-J.; You, X.-Z.; Huang, X.-Y. *Acta Crystallogr., Sect. C* **1996**, *52*.
(53) Tulip, T. H.; Corfield, P. W. R.; Ibers, J. A. *Acta Crystallogr., Sect. B* **1978**, *34*, 1549−1555.

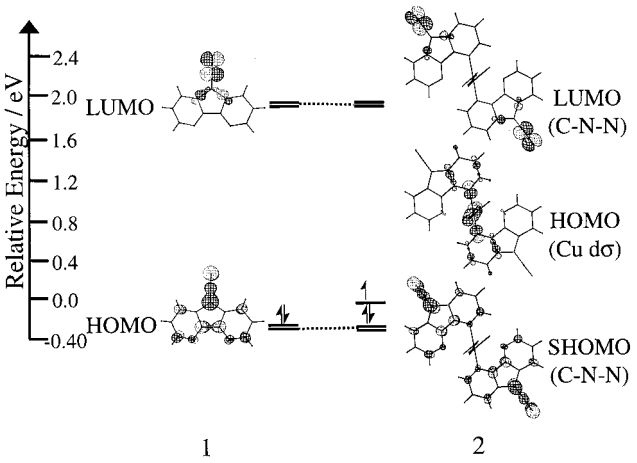

Figure 2. EHMO description of the frontier molecular orbitals of **1** and **2**. Since degenerate orbitals differ only in phase, only one MO is illustrated for each pair.

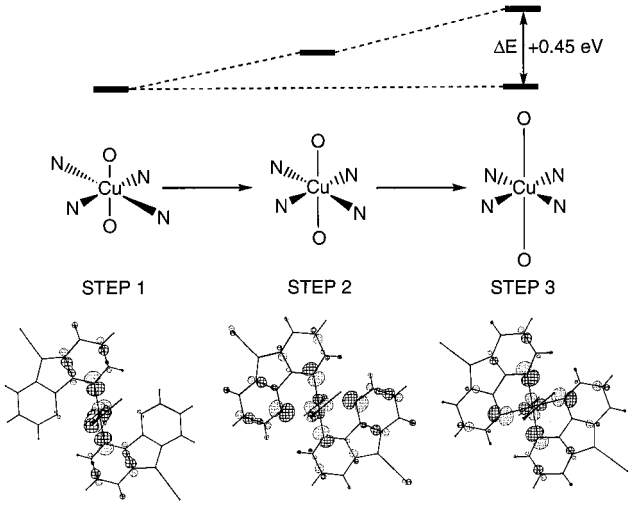

Figure 3. Energy changes associated with alteration of the coordination environment of **2** as derived from EHMO calculations.

To evaluate the unusual geometric structure of **2**, the EHMO calculations were performed at three different geometries for both **2** and the model compound $Cu(py)_4(NO_3)_2$ (Figure 3). For these calculations, the J−T axis was reoriented from the N−Cu−N vector to the O−Cu−O axis by rotating the chelating ligand of **2** until symmetric coordination was achieved. For $Cu(py)_4(NO_3)_2$, the geometry was altered by stepwise elongation of the Cu−O bond lengths and compression of one of the Cu−N vectors. For **2**, the overall energy of the system decreases by 0.45 eV when the J−T axis is directed along the N−Cu−N vector (Figure 3), even though the total overlap populations of the metal−ligand bonding orbitals remain nearly constant (Table 3). These results suggest that the geometry is a product of unfavorable steric interactions (i.e., between the hydrogen atoms at the α-carbons of the diimine ligands) rather than more favorable metal−ligand bonding interactions. This type of steric interaction is also thought to be partly responsible for the structural diversity observed for $Cu(bpy)_2^{2+}$ (bpy = 2,2′-bipyridine) complexes.[54] For $Cu(py)_4(NO_3)_2$, the overall energy of the system is lowered considerably (−1.3 eV) upon transition from the N-elongated structure to the symmetric O-elongated

(54) Hathaway, B. J.; Billing, D. E. *Coord. Chem. Rev.* **1970**, *5*, 143−207.

Table 3. Comparison of Bond Distances and Orbital Overlap Populations for **2** and $Cu(py)_4(NO_3)_2$ upon Rotation of the Cu(II) Jahn−Teller Axis

	2		$Cu(py)_4(NO_3)_2$	
bond/step	distance/Å	overlap population[a]	distance/Å	overlap population[a]
Cu−O/step 1	2.014	0.185	2.008	0.193
Cu−O/step 3	2.454	0.028	2.448	0.031
Cu−N (long)/step 1	2.652	0.033	2.630	0.047
Cu−N (long)/step 3	2.050	0.272	2.050	0.310
Cu−N (short)/step 1	1.982	0.358	2.066	0.312
Cu−N (short)/step 3	2.052	0.276	2.066	0.297

[a] Orbital population = $\sum 2nC_iC_jS_{ij}$ represents a decimal percentage of the total electron density that overlaps between all of the occupied atomic orbitals on atom x with all of the atomic orbitals on atom y summed over all occupied MOs.

geometry (steps 1−3). The effect is due primarily to an increase in the bonding orbital overlap populations along the three molecular axes. This increase in orbital overlap for the O-elongated geometry in $Cu(py)_4(NO_3)_2$ is not observed for **2** and is likely a reflection of the rigidity of the fluorene backbone, which restricts the orientation of the coordinating lone pairs and limits the ability of **1** to form strong bidentate σ-overlap. These results suggest that the lower energy structure of **2** is a result of a combination of effects: the slightly wider bite angle of the diimine skeleton and the inability of the planar diazafluorene backbone to reduce steric interactions with the adjacent ligand.

Solution Structure and Photochemistry. Solution Structure. Equatorial coordination of the nitrate counterions in **2** raises the potential for solvent molecules to occupy these sites in solution. Indeed, conductivity measurements confirm that upon dissolution of **2** in water, the complex forms a 2:1 electrolyte, indicating that water molecules occupy the equatorial coordination sites left vacant by the solvated counterions.[27]

The dissociation of the nitrate anions is further confirmed by solvent-dependent EPR spectra which show drastic variation when the glassing medium is altered. Two unique spectra are obtained in aqueous NaCl and H_2O:ethylene glycol (EG) media (Figure 4).[55] The EPR spectrum of **2** in aqueous NaCl (Figure 4a) indicates a 6-coordinate solution structure ($d_{x^2-y^2}$ ground state) with rhombic symmetry ($g_x = 2.10$, $g_y = 2.04$, $g_z = 2.23$, $A_z = 177 \times 10^{-4}$ cm^{-1}), as would be expected for a $CuN_2X_2N_2'$ system where X = halogen.[50] The *g*-values correlate well with those reported from single-crystal EPR studies of $Cu(dafone)_2X_2$ (dafone = 4,5-diazafluorene-9-one and X = Cl^-, Br^-), where the halide ions occupy the two equatorial coordination sites.[50]

Strong chloride binding is supported by the contrasting EPR spectrum of **2** in a frozen solution of H_2O:EG (1:20 v/v) which yields a mixture of two copper centers, both exhibiting a more axial symmetry (Figure 4b). The simulated spin-Hamiltonian parameters for the first (**2a**) species ($g_{xa} = 2.05$, $g_{ya} = 2.06$, $g_{za} = 2.29$, $A_{za} = 170 \times 10^{-4}$ cm^{-1}) suggest that the structure has near axial symmetry and N-rich coordination.[56−59] Structure

(55) Scans from 100 to 10 000 G have revealed no additional features, indicating that EPR-active spin-coupled dimeric species are not present.
(56) Menon, S.; Rajasekharan, M. V. *Inorg. Chem.* **1997**, *36*, 4983−4987.
(57) Pradilla, S. J.; Chen, H. W.; Koknat, F. W.; Fackler, J. P., Jr. *Inorg. Chem.* **1979**, *18*, 3519−3522.
(58) Benites, P. J.; Rawat, D. S.; Zaleski, J. M. *J. Am. Chem. Soc.* **2000**, *122*, 7208−7217.
(59) Astley, T.; Ellis, P. J.; Freeman, H. C.; Hitchman, M. A.; Keene, F. R.; Tiekink, E. R. T. *J. Chem. Soc., Dalton Trans.* **1995**, 595−601.

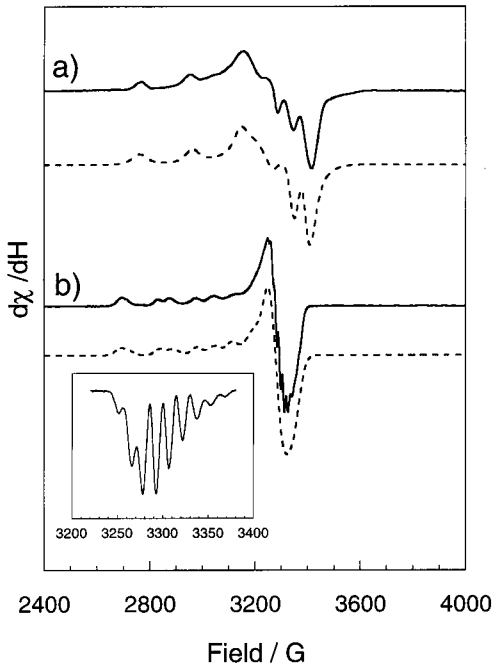

Figure 4. Observed EPR spectra (—) of **2** recorded at 77 K with corresponding simulations (- - -). (a) Aqueous NaCl (saturated) solution, and (b) a 20:1 mixture of ethylene glycol:water. Inset: Second derivative plot of $g_\perp$ transition.

2b is also near axial ($g_{xb} = 2.07$, $g_{yb} = 2.08$, $g_{zb} = 2.34$, $A_{zb} = 155 \times 10^{-4}$ cm^{-1}), but the increased g_z and decreased A_z values suggest a structure with increased oxygen coordination.[60] Despite the ~1:1 mixture of **2a**:**2b**, a clearly defined 9-line superhyperfine splitting pattern of the $g_\perp$ transition is also observed ($A_N = 15$ G), indicating symmetric coordination of both diazo−diazafluorene ligands in at least one of the two structures (Figure 4, inset). On the basis of these results, structure **2a** is best characterized as a CuN_4O_2 system where solvent (EG, 22 M) occupies the axial coordination positions, while **2b** more closely resembles that of $[Cu(dafone)_2(H_2O)_2](ClO_4)_2$ with H_2O (2.6 M) in the equatorial positions.[50] The structural assignment for **2a** is corroborated by the strong correlation of the spin-Hamiltonian parameters with crystallographically characterized $Cu(py)_4(O_2CCF_3)_2$, where the bulky triflate anion occupies the axial positions.[57] From the EMHO calculations, CuN_4 coordination in the equatorial plane is not expected to be the lowest energy structure for **2**. However, the nature of these calculations does not account for the lability of the nitrate counterions or the presence of a bulky coordinating solvent, which may provide sufficient driving force to induce a different solution structure.

Photochemistry. In the solid state, both **1** and **2** are photochemically unstable and decompose slowly under ambient light over the course of several days. Infrared measurements of solid-state photolysis of **2** (fluorolube or Nujol mulls) show complete disappearance of the diazo stretch in a period of 40 min ($\lambda \geq 455$ nm), suggesting that N_2 loss photochemistry associated with organic diazo analogues is conserved upon complexation to the copper center.

The electronic absorption spectrum of **1** in solution is characteristic of an aromatic diazo compound with a weak ($\epsilon = 41$ M^{-1}cm^{-1}) $n \rightarrow \pi^*$ transition of the diazo group ($\lambda_{max} = 480$ nm) that is not evident in the spectra of $Cu(dafone)_2$ derivatives (Figure 5).[27] In the electronic spectrum of **2**, the $n \rightarrow \pi^*$ transition from the diazo group remains energetically unperturbed, but exhibits an increase in the molar absorptivity due to the presence of two ligands per mole compound. The Cu(II) d−d transitions are observed as a single broad feature centered at 640 nm, consistent with a 6-coordinate mixed N,O coordination environment.[61] It is clear from this spectral analysis that photolysis of both **1** and **2** with $\lambda \geq 455$ nm results in the initial population of the ligand-based $n\pi^*$ state. In the previous report on the photonuclease activity of **2**, we noted both the increased activity of **2** relative to **1** and the evidence for the formation of Cu(I) during anaerobic photolysis ($\lambda \geq 455$ nm) of **2** in solution.[27] These observations led us to mechanistically evaluate the effects of Cu(II) upon the intermediates generated by $n \rightarrow \pi^*$ photolyses of **1** and **2**.

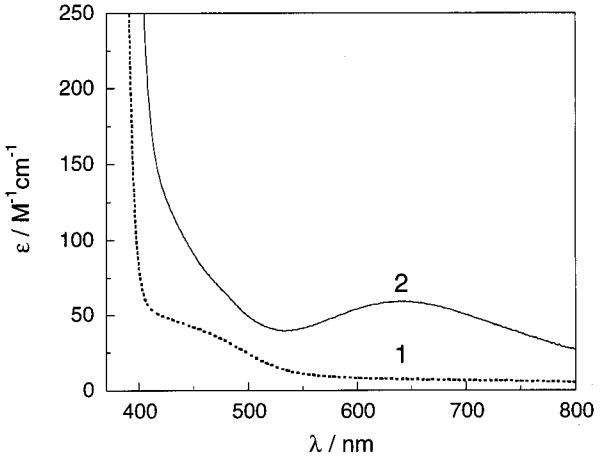

Figure 5. Electronic absorption spectra of **1** (MeOH) and **2** (H_2O).

Low-Temperature Photoreactivity. Matrix Photolysis of 1. Photolysis of **1** ($\lambda \geq 455$ nm) at 4 K in a 2-methyltetrahydrofuran (2-MeTHF) glass results in the formation of the triplet carbene derived from N_2 loss (Figure 6a). The zero field parameters (ZFS) ($|D/hc| = 0.408$ cm^{-1}, $|E/hc| = 0.0292$ cm^{-1}) are within the typical range expected for diaryl carbenes.[62] Interestingly, these values are nearly identical to those observed for fluorenylidene ($|D/hc| = 0.408$ cm^{-1}, $|E/hc| = 0.0283$ cm^{-1})[63] but are somewhat different than those reported for the positional isomers 9-diazo-1,8-diazafluorene[64] and 9-diazo-3,6-diazafluorene[65] ($|D/hc| = 0.442$ cm^{-1}, $|E/hc| = 0.029$ cm^{-1} and $|D/hc| = 0.438$ cm^{-1}, $|E/hc| = 0.0306$ cm^{-1}, respectively). Comparison of the ZFS parameters supports Schuster's assertion that the primary mechanism of the electronic perturbation introduced by the ring nitrogens is through bond rather than through space.[65]

Photolysis of **1** under the same conditions as above results in the growth of a series of electronic transitions in the visible region of the spectrum (Figure 6b). Previous reports of the electronic spectrum of fluorenylidene, both in a 2-MeTHF matrix at 10 K and in an acetonitrile solution at room

(60) Hathaway, B. J. In *Copper*; Wilkinson, G., Ed.; 1987; Vol. 5, pp 662−674.
(61) Lever, A. B. P.; Dodsworth, E. S. In *Electrochemistry, Charge-Transfer Spectroscopy, and Electronic Structure*; Solomon, E. I., Lever, A. B. P., Eds.; John Wiley & Sons: New York, 1999; Vol. 2, pp 227−287.
(62) Sander, W.; Bucher, G.; Wierlacher, S. *Chem. Rev.* **1993**, *93*, 1583−1621.
(63) Wasserman, E.; Trozzolo, A. M.; Yager, W. A.; Murray, R. W. *J. Chem. Phys.* **1964**, *40*, 2408−2410.
(64) Li, Y. Z.; Schuster, G. B. *J. Org. Chem.* **1986**, *51*, 3804−3811.
(65) Li, Y. Z.; Schuster, G. B. *J. Org. Chem.* **1987**, *52*, 3975−3979.

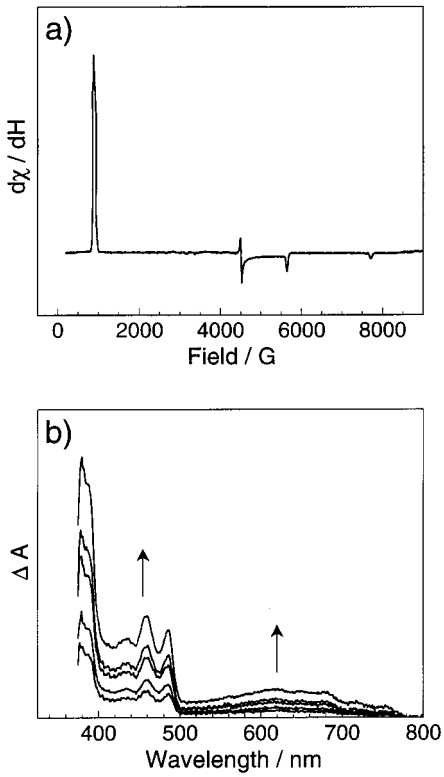

Figure 6. Spectral data acquired after the photolysis of **1** ($\lambda \geq 455$ nm) at 4 K in a 2-MeTHF glass. (a) EPR spectrum after 15 min of photolysis. (b) Difference electronic absorption spectra obtained after 10, 15, 20, 25, and 45 min photolysis periods.

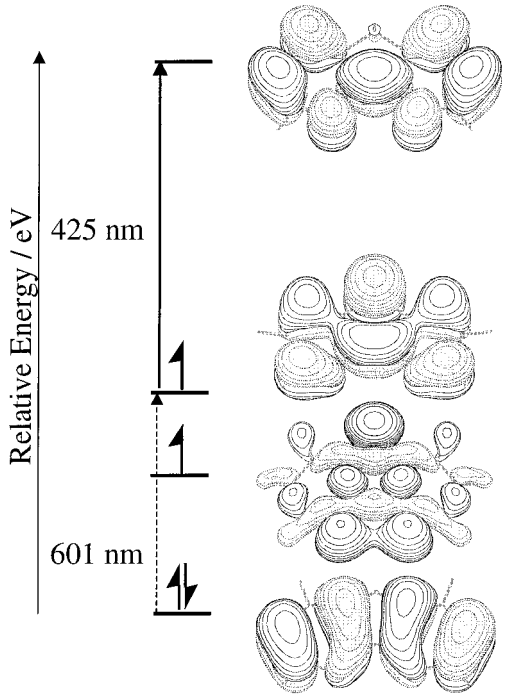

Figure 7. TDDFT description of the frontier molecular orbitals of 4,5-diazafluorenylidene.

temperature, cite absorption maxima at 440 and 470 nm with the latter being the more intense transition.[66−68] Our data closely parallel these results with a few subtle differences. The first is the appearance of a broad feature centered at 630 nm that has not previously been reported. Additionally, there are three prominent features (432, 457, and 485 nm) in the mid-visible spectral region. These maxima are spaced at ∼1260 cm^{-1}, suggesting vibrational coupling to a single electronic transition.

We have employed DFT and TDDFT methods to evaluate the electronic structure and electronic transitions for 4,5-diazafluorenylidene (Figure 6b) to confirm the identity of the intermediate observed at 4 K (Figure 6b). The geometric structure of 4,5-diazafluorenylidene was minimized in C_{2v} symmetry at the 6-31G** level using hybrid UB3LYP functionals. The calculated electronic structure of 4,5-diazafluorenylidene reveals a ground-state triplet with the two unpaired electrons in half-occupied, σ (in-plane) and π (out-of-plane) orbitals that are delocalized about the ring system. At the optimized geometry, TDDFT was used to calculate the five lowest energy spin-allowed electronic transitions for comparison to the experimental data. The lowest energy transition ($^3B_2 \leftarrow {}^3B_2$, ∼601 nm) is best described as delocalized $\pi \rightarrow \pi^*$ (LUMO) in origin with considerable electron density in the out-of-plane orbital at the 9-position (carbene) of the 4,5-diazafluorenylidene framework (Figure 7). Although spin-allowed, the transition is symmetry forbidden and therefore possesses low oscillator strength. The next lowest energy transition with appreciable oscillator strength is out-of-plane, half-occupied π (HOMO) → π^* in nature ($^3A_1 \leftarrow {}^3B_2$, ∼425 nm) in which the electron density at the carbene center is redistributed throughout the ring. Both the calculated 425 and 601 nm transitions are chemically reasonable and correspond well to those observed in Figure 6b. No other spin- or symmetry-allowed transitions with appreciable oscillator strengths were calculated to lie in this energy region.

The electronic structure calculation and corresponding normal coordinate analysis provide an opportunity to examine the molecular origin for the 1260 cm^{-1} vibration that couples to the $^3A_1 \leftarrow {}^3B_2$ transition centered near 450 nm. The normal coordinate analysis reveals six vibrations between 1260 and 1360 cm^{-1} that involve in-plane C−C breathing motions of the central ring in combination with C−H out-of-plane bending motions. By imposing the constraint that the electronic transition should be *y*-polarized in accordance with the symmetry selection rules in C_{2v}, only vibrations of a_1 symmetry would yield an allowed vibronic progression ($|\int \Psi_{el}\Psi_{vib}\hat{M}_{xyz}\Psi_{el}^{ex}\Psi_{vib}^{ex}\, d\tau|^2$). Since three vibrations of a_1 symmetry remain within this energy region and each involves in-plane C−C displacements of the central ring system, assignment of the progression to a particular normal mode cannot be made specifically, rather only in general.

Matrix Photolysis of 2. Photolysis of **2** ($\lambda \geq 455$ nm or $\lambda =$ 457 nm) at 4 K in a 1:20 H_2O:EG glass results in the growth of an isotropic radical signal concurrent with the loss of both of the Cu(II) EPR signals from **2a** and **2b** (Figure 8a). This spectrum is stable for hours at temperatures as high as 100 K and is in contrast to the carbene detected in the photolysis of **1** at 4 K (Figure 4a).[69] Three possible spin systems are plausible for a three-electron system. The first involves ferromagnetic

(66) Griller, D.; Hadel, L.; Nazran, A. S.; Platz, M. S.; Wong, P. C.; Scaiano, J. C. *J. Am. Chem. Soc.* **1984**, *106*, 2227−2235.
(67) Griller, D.; Montgomery, C. R.; Scaiano, J. C. *J. Am. Chem. Soc.* **1982**, *104*, 6813−6814.
(68) Grasse, P. B.; Brauer, B. E.; Zupancic, J. J.; Kaufmann, K. J.; Schuster, G. B. *J. Am. Chem. Soc.* **1983**, *105*, 6833−6845.

(69) It is possible that a carbene is formed and subsequently reacts; however, triplet fluorenylidene should, according to published Arrhenius parameters, be stable in alcohol and glycol matrixes at 4 K. See: Platz, et al. *J. Am. Chem. Soc.* **1992**, *114*, 4(3), 897−905.

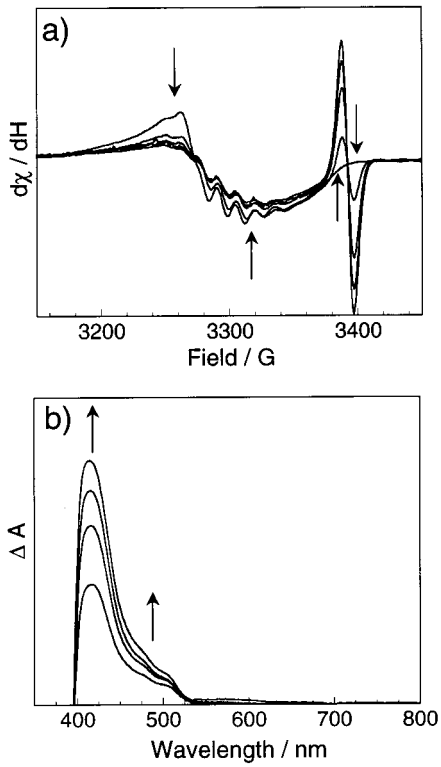

Figure 8. Spectral data following the photolysis of **2** ($\lambda = 457$ nm) at 77 K in a 20:1 ethylene glycol:water glass. (a) EPR spectra after 0, 5, 10, 15, and 20 min. (b) Difference electronic absorption spectra obtained after 3, 6, 9, and 12 min.

coupling of the ligand diradical to the spin centered on the Cu(II). This case would yield an $S = {}^3/_2$ spin system (↑····↓↓) with an EPR transition centered near $g \approx 4$, which is not observed. The second case can be described as a triplet ligand diradical antiferromagnetically coupled to Cu(II) (↓····↑↑), which should yield an EPR signal with $g_\perp > g_{||}$.[70] Last, a Cu(II) center that interacts with a singlet ligand diradical (↑····↑↓) would result in an unperturbed Cu(II) signal ($g_{||} > g_\perp$).[70] Neither of these latter two cases could be responsible for the observed spectrum, as they both retain characteristics of a Cu(II) EPR signal. Finally, a stepwise insertion reaction of the triplet carbene[71] with matrix to yield an uncoupled ligand−matrix radical pair, where the ligand spin is antiferromagnetically coupled to the Cu(II) center, could explain the observed EPR spectrum. This intermediate, however, is unlikely for a number of reasons. First, photolysis of **2** at 77 K yields the spectrum shown in Figure 8a. After warming the sample to room temperature anaerobically and subsequently recording the spectrum at 77 K, the organic radical vanishes, but the diminished Cu(II) signal remains unperturbed. Exposure of this sample to O_2 results in restoration of the Cu(II) signal intensity, thereby documenting the formation of Cu(I). Second, photolysis of **1** at 77 K in a 2:1 (v/v) 2-MeTHF:EG glass does not yield a $g = 2$ radical species that can be detected under our experimental conditions. This observation is consistent with the previously described reactivity of fluorenylidene at low temperatures,[72−75] which has shown that the

Scheme 2. Potential Photochemical Pathways to Radical Cation **3**

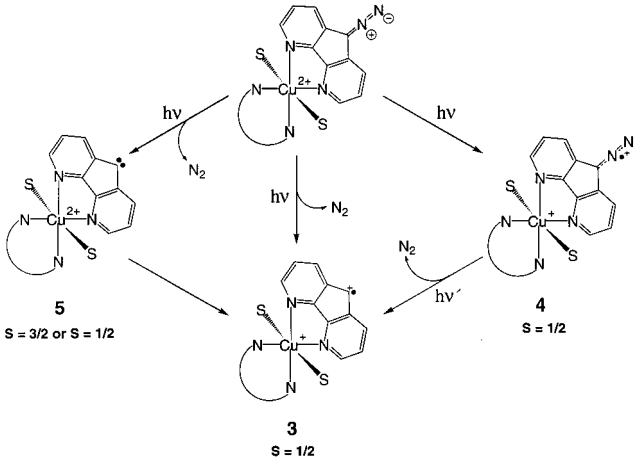

radical pair derived from the reaction with matrix is not stable at $T < 130$ K.[75] The absence of observable hyperfine coupling on the radical signal at $g = 2.0019$ infers a structure with the radical primarily localized on the carbon at the 9-position of the fluorene ring.[17−20,76,77] The absence of hyperfine coupling to N_2, which is commonly observed in one-electron oxidized diaryl diazo compounds,[17−20,76,77] confirms photoinduced N_2 loss along with reduction of the Cu(II) center and concomitant appearance of the monoradical signal. Therefore, the spectrum in Figure 8a is best described as a Cu(I)−$L^{\bullet+}$ intermediate (**3**) derived from the photoinduced oxidation of the diazo unit and subsequent N_2 loss to yield an overall $S = {}^1/_2$ spin system (Scheme 2).

This interpretation of the EPR results is further supported by the changes in the electronic absorption spectrum upon photolysis of **2** ($\lambda \geq 455$ nm) at 4 K in a 1:20 H_2O:EG glass. Difference electronic absorption spectra reveal the growth of a strong feature at 410 nm, with a shoulder to lower energy (Figure 8b). This absorption spectrum is nearly identical to those previously assigned to the carbene cation radicals of diaryl diazo derivatives formed upon oxidation and subsequent N_2 loss.[18−20,77] This spectrum is also different than that expected for a simple 9-fluorenyl radical, which exhibits an absorption maximum at 500 nm.[68,78] Together the EPR and electronic spectra identify the photogenerated intermediate at 4 K as a Cu(I)−$L^{\bullet+}$ species resulting from intramolecular electron transfer and N_2 loss.

Discussion

The solid-state structure of **2** is unusual in that the nitrate counterions, which may be expected to be weakly bound in a bis(chelate) stoichiometry (i.e., along the J−T axis), provide stronger equatorial ligation than the diimine ligand. Generation of a 2:1 electrolyte upon dissolution of **2** reveals the ability to generate open, and potentially strong, coordination positions for chemical or biological solution substrates such as DNA.[27]

(70) Chaudhuri, P.; Verani, C. N.; Bill, E.; Bothe, E.; Weyhermueller, T.; Wieghardt, K. *J. Am. Chem. Soc.* **2001**, *123*, 2213−2223.
(71) Platz, M. S. In *The Chemistry, Kinetics, and Mechanisms of Triplet Carbene Processes in Low-Temperature Glasses and Solids*; Platz, M. S., Ed.; Plenum: New York, 1990; pp 143−211.
(72) Moss, R. A.; Joyce, M. A. *J. Am. Chem. Soc.* **1978**, *100*, 4475−4480.
(73) Wright, B. B.; Platz, M. S. *J. Am. Chem. Soc.* **1984**, *106*, 4175−4180.
(74) Leyva, E.; Barcus, R. L.; Platz, M. S. *J. Am. Chem. Soc.* **1986**, *108*, 7786−7788.
(75) Ruzicka, J.; Leyva, E.; Platz, M. S. *J. Am. Chem. Soc.* **1992**, *114*, 897−905.
(76) Ishiguro, K.; Sawaki, Y.; Izuoka, A.; Sugawara, T.; Iwamura, H. *J. Am. Chem. Soc.* **1987**, *109*, 2530−2531.
(77) Kato, N.; Miyazaki, T.; Fueki, K.; Kobayashi, N.; Ishiguro, K.; Sawaki, Y. *J. Chem. Soc., Perkin Trans. 2* **1987**, 881−884.
(78) Alberti, A.; Griller, D.; Nazran, A. S.; Pedulli, G. F. *J. Am. Chem. Soc.* **1986**, *108*, 3024−3028.

Moreover, the fluxionalities of these coordination sites and the ability of the diazafluorene skeleton to adopt more than one geometric disposition about the metal give complexes of this type significant structural flexibility.

From the electronic spectra of **1** and **2** (Figure 5) and the frontier molecular orbital description (Figure 2), photoexcitation of **1** and **2** with $\lambda \geq 455$ nm initially populates a ligand localized, diazo-centered excited state that has propensity for N_2 loss due to the N═N nonbonding and C═N bonding to N═N antibonding and C═N nonbonding nature of the transition. In the absence of metal, N_2 loss and subsequent formation of a triplet carbene intermediate are observed. However, in the presence of Cu(II), an excited state intramolecular redox reaction occurs, which leads directly to a $S = {}^1/_2$ Cu(I)−$L^{\bullet+}$ (↑↓•••↑) species without detection of the Cu(I)−L═$N_2^{\bullet+}$ diazo cation radical (**4**) ($\lambda_{max} \approx 680$ nm).[18−20,76] This reaction pathway is the most viable as direct photoinduced N_2 loss would produce a carbene (**5**) that energetically cannot be oxidized by the modest redox potential of Cu(II).[79] Moreover, fluorescence quantum yield measurements illustrate that Cu(II) significantly quenches the photochemically prepared excited state ($\phi_{f1} = 0.230$ vs $\phi_{f2} = 0.021$) by either energy transfer to ligand field states or direct electron transfer via oxidation of the diazo unit. The viability of the electron-transfer pathway is clear if the energy of the charge-separated state is estimated by the ΔE (redox) approximation.[61,80] The positive Cu^{2+}/Cu^{+} redox couple ($E_{1/2} = +0.1$ V vs SCE) and the modest $\mathbf{1}/\mathbf{1}^{\bullet+}$ ligand redox potential ($E_{1/2} = +1.4$ V vs SCE, irreversible) places the charge-separated state at $\Delta E \approx 1.3$ V above the ground state. Photoexcitation with $\lambda = 457$ nm provides ∼2.7 V of excited-state potential which is sufficient to drive an intramolecular redox reaction.

Formation of the $S = {}^1/_2$ Cu(I)−$L^{\bullet+}$ (↑↓•••↑) intermediate contrasts the work of Iwamura et al. which demonstrates that the ligand diradical prepared upon photoinduced ($\lambda = 532$ nm, 2.33 eV) loss of N_2 from an analogous [Cu(diazodi-4-pyridylmethane)$(hfac)_2]_n$ construct ferromagnetically couples to the Cu(II) spin to yield a local $S = {}^3/_2$ spin (↑•••↑↑) system.[22] These spin centers interact ferromagnetically along the polymeric chain to produce a transient magnetic material with a net $S = 33.6$ spin state over the sample. Interestingly, no photoinduced redox process occurs to yield the isoelectronic $S = {}^1/_2$ Cu(I)−$L^{\bullet+}$ (↑↓•••↑) intermediate. The difference in the photogenerated intermediates between **2** and the [Cu(diazodi-4-pyridylmethane)$(hfac)_2]_n$ system can only be rationalized by assuming that the Cu(I)−$L^{\bullet+}$ (↑↓•••↑) state energy lies above the 532 nm photoexcitation energy. Given the 6-coordinate, octahedral geometry about the Cu(II) center in [Cu(diazodi-4-pyridylmethane)$(hfac)_2]_n$ and the fact that the charge on the metal is neutralized by the hfac counterions, photoinduced formation of Cu(I) in the solid state (i.e., absence of solvation) may indeed require excitation energy that exceeds 2.33 eV.

The formation of intermediate **3** ($S = {}^1/_2$ Cu(I)−$L^{\bullet+}$, ↑↓•••↑) also has general implications to the identities of redox active metal−ligand radical intermediates generated during turnover of metalloenzymes such as galactose oxidase. First, the nature of the intermediate itself is chemically unusual relative to one-electron, ground-state oxidation pathways, which typically lead to generation of a Cu(II) center prior to ligand radical formation. This is due to the disparate ease in oxidizing Cu(I) relative to stable organic ligands. Second and within this theme, Cu(II)−phenoxyl models of the active form of galactose oxidase have been generated electrochemically and show that the ligand localized π-monoradical is antiferromagnetically coupled to the lone electron in the $d_{x^2-y^2}$ orbital to yield a net $S = 0$ spin.[34] Analogously, the active form of the enzyme is prepared by two sequential one-electron oxidations of the Cu(I)−tyrosine resting state by O_2 to yield a Cu(II)−tyrosyl radical, where the first step is oxidation of the Cu(I) center. The negative Cu(II)/Cu(I) redox potential (∼−0.3 to −0.5 V vs NHE),[33] which derives partially from the distorted square planar geometry that favors the Cu(II) oxidation state, is therefore responsible for metal (Cu(II)−tyrosine) and not ligand (Cu(I)−tyrosine•) oxidation as the first step in the mechanism.

Conclusions

Our results show that the unusual structure of **2** in the solid state derives from the enlarged bite angle of the fluorene skeleton and steric interactions between the adjacent hydrogen atoms in the symmetrically coordinated state. This is in contrast to $Cu(py)_4(NO_3)_2$ which possesses a more stable structure with the nitrate counterions bound along the Jahn−Teller axis. Despite the strong coordination of the counterions, solvent-dependent EPR studies confirm that the nitrates dissociate to yield 6-coordinate $CuN_2X_2N_2'$ structures with either a bound chloride ion or a mixture of counterion and solvent. Photolyses of **1** and **2** result in N_2 loss and formation of either carbene or Cu(I)−$L^{\bullet+}$ intermediates, respectively. The metal−ligand radical intermediate is chemically unusual relative to one-electron ground-state oxidation pathways which typically lead to generation of a Cu(II) center prior to ligand radical cation formation. Finally, the excited-state redox reaction which leads to the Cu(I)−$L^{\bullet+}$ intermediate is different that that observed upon photolysis of the analogous [Cu(diazodi-4-pyridylmethane)-$(hfac)_2]_n$ system, thereby illustrating the important role redox active transition metals play in determining the nature of fundamental metal−ligand radical intermediates.

Acknowledgment. We thank Aurora Clark and Prof. Joe Gajewski for helpful discussions. The generous support of the American Cancer Society (RPG-99-156-01-C), the donors of the Petroleum Research Fund (PRF #33340-G4), administered by the American Chemical Society, and the Research Corporation (Research Innovation Award #RI0102 for J.M.Z.) are gratefully acknowledged.

Supporting Information Available: Atomic coordinates, bond lengths, and bond angles (PDF). This material is available free of charge via the Internet at http://pubs.acs.org.

JA0120072

(79) Muchall, H. M.; Werstiuk, N. H.; Choudhury, B. *Can. J. Chem.* **1998**, *76*, 221−227.
(80) Vlcek, A. A. E. A. *Electrochim. Acta* **1968**, *13*, 1063−1078.